

Tracing the source of oxidizing fluids in subduction zones using iron isotopes in garnet

Anna R. Gerrits^{1*}, Edward Inglis², Besim Dragovic³, Paul G. Starr¹, Ethan F. Baxter^{1*}, Kevin Burton⁴

¹Department of Earth and Environmental Sciences, Boston College, 140 Commonwealth Avenue, Chestnut Hill, MA 02467, USA

²Institut de Physique du Globe de Paris, Sorbonne Paris Cité, CNRS, 1 rue Jussieu, 75238, Paris cedex 05, France

³Department of Geosciences, Boise State University, 1910 University Drive, Boise, ID 83725, USA

⁴Department of Earth Sciences, Durham University, Science Labs, Durham, DH1 3LE, UK

*Corresponding authors

Subduction zones are the primary areas of chemical and mass transfer between the Earth's surface and the mantle. During subduction, the down going plate carries oxidized material into the mantle and releases large amounts of water through the breakdown of hydrous minerals^{1,2}. This dehydration has been linked to subduction seismicity³, arc volcanism^{1,4,5}, and redox (fO_2) changes in the subducting slab and overlying mantle wedge⁶⁻¹⁰. Despite this, no petrologic record from the source of oxidizing (high- fO_2) fluids from the down going slab has yet been observed. Recent work has demonstrated that the release of oxidizing species, such as sulfur (S), from the subducting slab may play a key role in controlling subduction zone redox processes¹¹ and occurs coincident with fluid release associated with the breakdown of hydrous mineralogy such as lawsonite across the blueschist-eclogite facies transition¹². Here we show a record of progressive syn-dehydration redox change recorded in zoned garnet crystals from Sifnos, Greece that grew through lawsonite breakdown during subduction ca. 45 million years ago. Oxygen fugacities (fO_2), calculated using garnet-epidote oxybarometry for multiple growth zones within single garnet grains, have been coupled with stable Fe isotope compositions in the same growth zones. These combined measurements reveal that garnet interiors grew under relatively oxidized conditions, recording higher fO_2 and lower $\delta^{56}Fe$ values, whereas garnet rims record more reduced conditions with lower fO_2 and higher $\delta^{56}Fe$ values; this shift occurs during lawsonite dehydration, as shown by thermodynamic analysis. These data show that the redox state of the residual mineral assemblages within the slab became more reduced during progressive subduction zone dehydration. This is consistent with the hypothesis that lawsonite dehydration accompanied by the release of oxidizing

species, such as sulfate, plays an important and measurable role in the global redox budget and provides a valuable contribution to sub-arc mantle oxidation.

Oxygen fugacity (fO_2), the chemical potential of oxygen in a system, is an intensive thermodynamic property that controls the speciation of multi-valent elements, such as iron, which regulates the ability of these elements to contribute to mineral forming reactions¹³. Because of this, fO_2 is an important chemical control in a given environment, such as a subduction zone, where the subducting slab experiences multiple changes in mineral assemblages as a result of changes in pressure-temperature (P - T) conditions. During subduction, components of the downgoing lithosphere, including sediments, altered mafic oceanic crust, and serpentinized mantle, carry water and other volatiles into the subduction zone. It is widely accepted that while there is significant fluid loss during shallow subduction, hydrous phases in the downgoing slab, such as lawsonite, chlorite, chloritoid, phengite, and serpentine retain water to greater depths^{1,2,14}. Lawsonite, $CaAl_2Si_2O_7(OH)_2 \cdot H_2O$, is a common hydrous mineral in mafic oceanic crust and contains ~12 wt% water,^{1,2,14} making the metamorphic destabilization of lawsonite an important fluid-producing reaction within subduction zones. Much debate exists about the role of slab-derived fluids in oxidizing the overlying sub-arc mantle and how such fluids can be used to explain the oxidized and volatile-rich signatures observed in arc magmas relative to their MORB or OIB counterparts^{1,4-10,15}. The role of strongly oxidizing sulfur in governing subduction zone redox processes has received much attention^{7,9,11,12} and recent work has suggested that the release of oxidizing sulfur species, predominantly from the breakdown of sulfates, may occur across the blueschist-eclogite facies transition, coincident with the breakdown of hydrous phases such as chlorite, talc and lawsonite¹². Evaluation of redox-budget fluxes from the subducting slab suggests that the release of sulfate, in fluids from the subducting slab, may play a key role in generating the elevated fO_2 values proposed for the sub-arc mantle^{12,16}. Here we present a novel geochemical method on the scale of individual mineral growth zones to document the redox nature of the fluids released during key subduction dehydration events.

To identify the source of these oxidizing (high- fO_2) fluids, we use the exhumed rock record to constrain the fO_2 of the residual slab mineral assemblage, which records redox changes resulting from

dehydration reactions. There exist limited tools with which to measure the fO_2 of the residual slab assemblages. Recent work has demonstrated the utility of garnet as a robust recorder of changing conditions during its formation and growth, often spanning millions of years¹⁷⁻¹⁹. Here we present the first high precision stable Fe isotope measurements of individual garnet growth zones to examine the evolving fO_2 of the down-going slab during subduction. Changes in oxidation state are manifested in the $Fe^{3+}/\Sigma Fe$ ratio of minerals and result in a redox driven fractionation of Fe isotopes, as heavier Fe isotopes (higher $\delta^{56}Fe$ values) are preferentially incorporated in bonds involving Fe^{3+} relative to Fe^{2+} when the system is in equilibrium^{20,21}. Previous work on slab serpentinites has suggested that subducting slab material will lose isotopically light iron with increasing grade, as a result of the release of fluids enriched in Fe^{2+} in the form of aqueous $Fe^{2+}-SO_x$, $Fe^{2+}-Cl_2$, and $Fe^{2+}-CO_x$ complexes²². Despite this, no such effect has been resolvable on a whole rock scale for meta-mafic lithologies within subduction zones²³. In our study, iron isotope measurements are coupled with garnet-epidote oxygen barometry calculations²⁴, using multiple epidote inclusions sampled radially within a single garnet grain (Fig.1), to provide a record of fO_2 change during garnet growth. This study proposes the use of the relationship between the oxidation state and the isotopic composition of Fe recorded at the mineral scale, within zoned garnet crystals, as a tracer of fO_2 change and the release of fluids containing oxidizing species during metamorphic devolatilization of subducting oceanic crust.

Applying these methods, we present Fe isotope data and oxygen fugacity calculations (Figs. 1,2) for three zoned garnet crystals hosted within subducted and exhumed metabasalts from Sifnos, Greece. Plotting fO_2 as $\Delta\log FMQ$ against $\delta^{56}Fe$ for samples 09DSF-23E and 09DSF-54A illustrated in Fig. 2, shows a significant change from more oxidized garnet interiors (higher $\Delta\log FMQ$) with a lighter Fe isotope signature (lower $\delta^{56}Fe$) isotopes to more reduced garnet rims (lower $\Delta\log FMQ$) with a higher $\delta^{56}Fe$ compositions. Sample 06MSF-6C shows no significant change in calculated fO_2 ($\Delta\log FMQ$) values from garnet interior to rim and only a minor variation in $\delta^{56}Fe$, with lower $\delta^{56}Fe$ values in the garnet core than in the garnet rim (Fig. 2). Oxygen fugacity values calculated here are consistent with the typical

range of subducted metabasaltic fO_2 values²⁴⁻²⁷ in that they show more oxidized conditions, relative to the fayalite-magnetite-quartz (FMQ) buffer, than unaltered mid-ocean ridge basalt (MORB)⁷. The data from the intermediate garnet zones of sample DSF-23E allow for the possibility of a small increase in $\Delta\log\text{FMQ}$ before the sharp drop to the rim. We can only speculate on the cause of this possible increase; perhaps this reflects the influx of an oxidizing fluid from a deeper dehydrating assemblage as it passes through the system. Regardless, the key result from our data is the sharp drop in fO_2 from garnet interior zones to the rim: a drop that coincides with a sharp increase in $\delta^{56}\text{Fe}$ values.

These data show that there is significant redox change recorded in the mafic component of the slab during subduction at the mineral scale. In order to explore the possible link between these redox changes recorded in garnet and key dehydration reactions, thermodynamic modelling constraints on the P - T evolution of these samples are shown in Fig. 3 and Supplementary Figures 6 and 7. For samples 09DSF-23E (Fig. 3) and 09DSF-54A (Supplementary Figure 6), garnet growth spanned the onset of lawsonite breakdown along subduction zone P - T paths for Sifnos, Greece^{18,19,28}. To the contrary, garnets in sample 06MSF-6C likely ceased growing prior to lawsonite breakdown (Supplementary Figure 7 and Dragovic et al., 2012). This suggests that processes operating during the breakdown of lawsonite are responsible for causing the change in fO_2 from garnet interior zones to the rim recorded in 09DSF-23E and 09DSF-54A. These observations support the hypothesis that the dehydration of lawsonite plays a key role in liberating fluids, which can then become carriers of oxidizing species, thus altering the redox state of the subducting metamorphic mineral assemblage. Overall, our data reveal that garnet interiors grew under relatively oxidized conditions, recording higher fO_2 and lower $\delta^{56}\text{Fe}$ values, whereas garnet rims record more reduced conditions with lower fO_2 and higher $\delta^{56}\text{Fe}$ values with this shift occurring during lawsonite dehydration.

While bulk rock $\text{Fe}^{3+}/\Sigma\text{Fe}$ ratios can become decoupled from fO_2 , the observed inverse relationship from garnet interiors to rims between increasing $\delta^{56}\text{Fe}$ values and decreasing fO_2 (Fig. 1D) confirms that Fe isotope fractionation is linked to changing redox conditions. To account for the observed

covariation between higher fO_2 and lower $\delta^{56}Fe$ in garnet interiors relative to lower fO_2 and higher $\delta^{56}Fe$ in garnet rims, we propose two possible mechanisms related to the release of oxidizing fluids. First, iron isotope fractionation occurs as an open system process, controlled by the solubility difference between Fe^{2+} and Fe^{3+} . The higher solubility of Fe^{2+} relative to Fe^{3+} promotes Fe isotope fractionation as lighter Fe isotopes are complexed into oxidizing fluids, in the form of $Fe^{2+}-SO_x$ and $Fe^{2+}-CO_x$ complexes which are subsequently removed from the system. The progressive removal of Fe^{2+} bearing, isotopically light fluids is recorded by prograde garnet growth in the residual source rock, and can explain the shift from light to heavy Fe isotope compositions between garnet interiors and rims. In this scenario, the iron isotopes act as a tracer of the release of oxidizing species, with which Fe^{2+} preferentially complexes, within fluids released during the breakdown of hydrous mineralogy.

A second, complementary mechanism is that Fe isotope fractionation is controlled by the bulk rock $Fe^{3+}/\Sigma Fe$ ratio in a closed system with respect to Fe, with changing oxygen fugacity. Fluids charged with oxidizing species leave the system, reducing the fO_2 of the system, and leaving behind a more reduced residual mineral assemblage enriched in Fe^{2+} . This fO_2 change does not alter the whole rock Fe isotope composition, but instead, as garnet more readily incorporates isotopically light Fe^{2+} , causes a shift towards higher $\delta^{56}Fe$ values within garnet crystal rims due to simple Rayleigh fractionation. In this case, the iron isotopes act as a more direct tracer of the changing bulk rock $Fe^{3+}/\Sigma Fe$ ratio and fO_2 . While it is difficult to determine which is the dominant mechanism responsible for the observed Fe isotope fractionation, it is plausible that during garnet growth a combination of these two mechanisms could contribute, as both are driven by the release of oxidizing fluids during progressive dehydration.

The large drop change in fO_2 ($\Delta \log FMQ$) and increase in $\delta^{56}Fe$ values observed towards the garnet rim in samples 09DSF-23E (Fig. 1&2) and 09DSF-54A (Fig. 2), coincides with the interval of lawsonite breakdown and release of a free fluid phase as shown by thermodynamic modeling (Fig. 3 and Supplementary Figure 6). Whilst the lawsonite breakdown reaction itself did not directly create the oxidizing nature of those fluids, thermodynamic modelling has shown that the sulfate mineral, anhydrite

(CaSO₄), undergoes destabilization around the blueschist to eclogite transition at the same P - T conditions as the breakdown of lawsonite¹². As a result, it is suggested that fluids produced during lawsonite dehydration could be charged with SO_x complexes released from the coincident breakdown of anhydrite in neighboring lithologies, and thus serve as a powerful oxidant within these fluids. This hypothesis is fully supported by the trends in the Fe-isotope and fO_2 data, as light Fe is preferentially removed as Fe²⁺-SO_x complexes²⁹, leaving a progressively more reduced residual assemblage. We conclude that this data supports the hypothesis that the breakdown of lawsonite during subduction produces a fluid that influences the redox state and iron isotopic signatures of the subducting mafic slab, which plays an important role in the overall global redox budget. In addition, this study provides the first evidence that Fe isotope variations in zoned garnets are a sensitive recorder of dehydration-driven redox change occurring during metamorphism of subducting oceanic lithosphere.

Much debate exists about the cause of volatile enrichment and oxidized nature of arc magmas^{1,4-10,15}. It is widely accepted that fluids released from the subducting slab are responsible for altering the sub-arc mantle, the source region for arc magmas. A number of studies propose that these fluids, originating from dehydration of oceanic sediments, mafic crust, and serpentinized mantle, are the agents of mantle wedge oxidation and have shown that the transfer of oxidizing species from the slab to the sub-arc mantle within these metamorphic fluids are capable of causing significant shifts in the fO_2 of the sub-arc mantle^{7,9,10}. Alternatively, it has been suggested that the oxidation of arc magmas may occur during magmatic differentiation or degassing^{15,16}. This study provides evidence for redox change in the mafic component of the downgoing slab inferred to be the result of the release of oxidizing fluids during lawsonite breakdown. By fingerprinting the source of oxidizing (high- fO_2) fluids in the subducting slab, our study provides support for the idea that slab-derived fluids play an important role in the oxidation of the sub-arc mantle and related arc volcanic magmas.

References

1. Schmidt, M. W. & Poli, S. Experimentally based water budgets for dehydrating slabs and consequences for arc magma generation. *Earth Planet. Sci. Lett.* **163**, 361–379 (1998).
2. Magni, V., Bouilhol, P. & van Hunen, J. Deep water recycling through time. *Geochemistry Geophys. Geosystems* **15**, 4203–4216 (2014).
3. Okazaki, K. & Hirth, G. Dehydration of lawsonite could directly trigger earthquakes in subducting oceanic crust. *Nature* **530**, 81–84 (2016).
4. Tatsumi, Y. Formation of the volcanic front in subduction zones. *Geophys. Res. Lett.* **13**, 717–720 (1986).
5. Marschall, H. R. & Schumacher, J. C. Arc magmas sourced from mélangé diapirs in subduction zones. *Nat. Geosci.* **5**, 862–867 (2012).
6. Breeding, C. M., Ague, J. J. & Bröcker, M. Fluid-metasedimentary rock interactions in subduction-zone mélangé: Implications for the chemical composition of arc magmas. *Geology* **32**, 1041–1044 (2004).
7. Kelley, K. A. & Cottrell, E. Water and the Oxidation State of Subduction Zone Magmas. *Science (80-.)*. **325**, 605–607 (2009).
8. Parkinson, I. J. & Arculus, R. J. The redox state of subduction zones: Insights from arc-peridotites. *Chem. Geol.* **160**, 409–423 (1999).
9. Evans, K. A., Elburg, M. A. & Kamenetsky, V. S. Oxidation state of subarc mantle. *Geology* **40**, 783–786 (2012).
10. Debret, B. & Sverjensky, D. A. Highly oxidising fluids generated during serpentinite breakdown in subduction zones/704/2151/209/704/2151/431/119/118 article. *Sci. Rep.* **7**, 1–6 (2017).
11. Pons, M.-L., Debret, B., Bouilhol, P., Delacour, A. & Williams, H. Zinc isotope evidence for sulfate-rich fluid transfer across subduction zones. *Nat. Commun.* **7**, 13794 (2016).
12. Tomkins, A. G. & Evans, K. A. Separate Zones of Sulfate and Sulfide Release from Subducted

- Mafic Oceanic Crust. *Earth Planet. Sci. Lett.* **428**, 73–83 (2015).
13. Frost, R. B. Introduction to oxygen fugacity and its petrologic importance. in *Reviews in Mineralogy* (ed. Lindsley, D. H.) **25**, 1–9 (1991).
 14. Poli, S. & Schmidt, M. W. H₂O transport and release in subduction zones: Experimental constraints on basaltic and andesitic systems. *J. Geophys. Res. Solid Earth* **100**, 22299–22314 (1995).
 15. Lee, C. T. A. *et al.* The redox state of arc mantle using Zn/Fe systematics. *Nature* **468**, 681–685 (2010).
 16. Evans, K. A. The redox budget of subduction zones. *Earth-Science Rev.* **113**, 11–32 (2012).
 17. Baxter, E. F. & Caddick, M. J. Garnet growth as a proxy for progressive subduction zone dehydration. *Geology* **41**, 643–646 (2013).
 18. Dragovic, B., Baxter, E. F. & Caddick, M. J. Pulsed dehydration and garnet growth during subduction revealed by zoned garnet geochronology and thermodynamic modeling, Sifnos, Greece. *Earth Planet. Sci. Lett.* **413**, 111–122 (2015).
 19. Dragovic, B., Samanta, L. M., Baxter, E. F. & Selverstone, J. Using garnet to constrain the duration and rate of water-releasing metamorphic reactions during subduction: An example from Sifnos, Greece. *Chem. Geol.* **314–317**, 9–22 (2012).
 20. Polyakov, V. B. & Mineev, S. D. The use of Mossbauer spectroscopy in stable isotope geochemistry. *Geochim. Cosmochim. Acta* **64**, 849–865 (2000).
 21. Schauble, E. A., Rossman, G. R. & Taylor, H. P. Theoretical estimates of equilibrium Fe-isotope fractionations from vibrational spectroscopy. *Geochim. Cosmochim. Acta* **65**, 2487–2497 (2001).
 22. Debret, B. *et al.* Isotopic evidence for iron mobility during subduction. *Geology* **44**, 215–218 (2016).
 23. Inglis, E. C. *et al.* The behavior of iron and zinc stable isotopes accompanying the subduction of mafic oceanic crust: A case study from Western Alpine ophiolites. *Geochemistry, Geophys. Geosystems* **18**, 2562–2579 (2017).

24. Donohue, C. L. & Essene, E. J. An oxygen barometer with the assemblage garnet-epidote. *Earth Planet. Sci. Lett.* **181**, 459–472 (2000).
25. Boundy, T. M., Donohue, C. L., Essene, E. J., Mezger, K. & Austrheim, H. Discovery of eclogite facies carbonate rocks from the Lindås Nappe, Caledonides, Western Norway. *J. Metamorph. Geol.* **20**, 649–667 (2002).
26. Cao, Y., Song, S. G., Niu, Y. L., Jung, H. & Jin, Z. M. Variation of mineral composition, fabric and oxygen fugacity from massive to foliated eclogites during exhumation of subducted ocean crust in the North Qilian suture zone, NW China. *J. Metamorph. Geol.* **29**, 699–720 (2011).
27. Mattinson, C. G., Zhang, R. Y., Tsujimori, T. & Liou, J. G. Epidote-rich talc-kyanite-phengite eclogites, Sulu terrane, eastern China: P-T-fo₂ estimates and the significance of the epidote-talc assemblage in eclogite. *Am. Mineral.* **89**, 1772–1783 (2004).
28. Groppo, C., Forster, M., Lister, G. & Compagnoni, R. Glaucophane schists and associated rocks from Sifnos (Cyclades, Greece): New constraints on the P-T evolution from oxidized systems. *Lithos* **109**, 254–273 (2009).
29. Hill, P. S., Schauble, E. A. & Young, E. D. Effects of changing solution chemistry on Fe³⁺/Fe²⁺ isotope fractionation in aqueous Fe-Cl solutions. *Geochim. Cosmochim. Acta* **74**, 6669–6689 (2010).

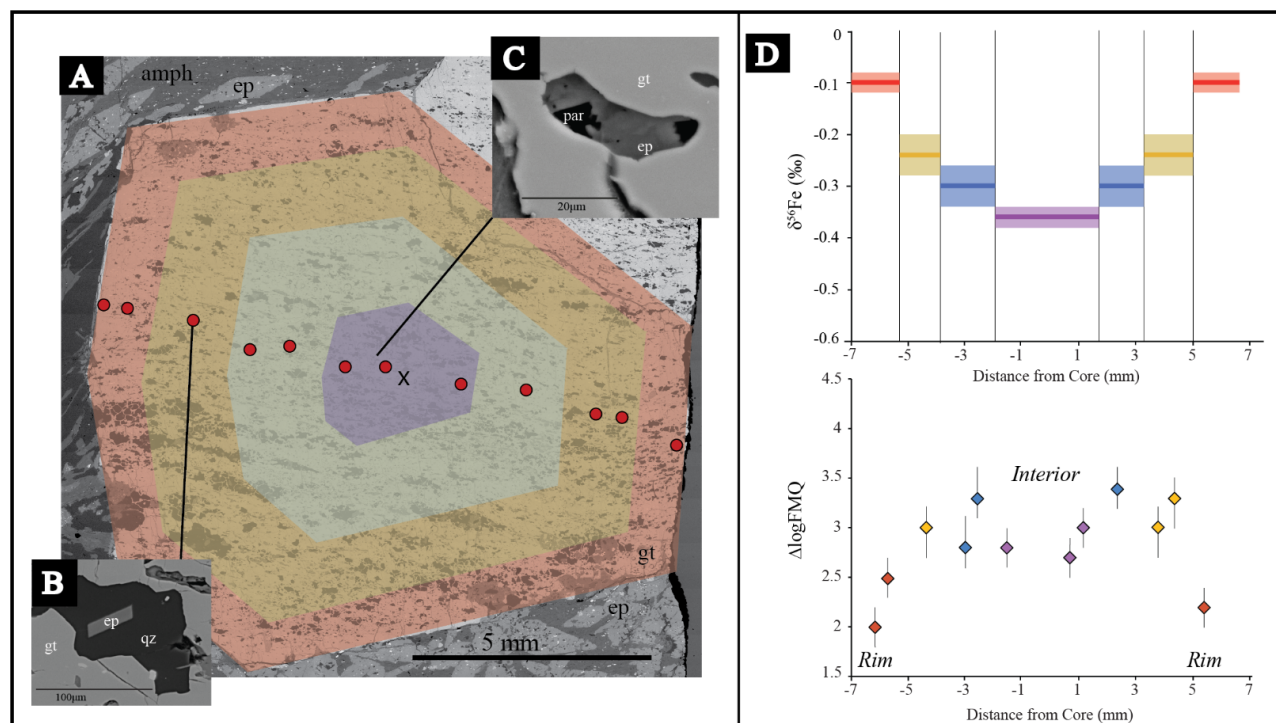


Figure 1 – A) BSE image of the garnet grain used for Fe isotope and oxybarometry analysis in sample 09DSF-23E. Epidote inclusions used in oxybarometry calculations are shown as red circles and sampling zones used for iron isotope measurements indicated by colored regions. B) Example of an epidote inclusion used in oxybarometry calculations. C) Example of a lawsonite pseudomorph that was avoided in oxybarometry calculations. D) $\delta^{56}\text{Fe}$ (top) and $\Delta\log\text{FMQ}$ (bottom) values for sample 09DSF-23E plotted from garnet rim to rim. $\delta^{56}\text{Fe}$ values were analyzed once for each garnet zone and have been plotted symmetrically to show trends from garnet rim to rim with measurements plotted as solid lines with associated errors indicated by the shaded regions. Error calculations for the $\delta^{56}\text{Fe}$ data are the two-standard deviation of four isotopic analysis for each sample. Errors for the $\Delta\log\text{FMQ}$ values are ± 0.2 log units for the core (purple) and rim (red) points, calculated using the ± 1 kbar and $\pm 40^\circ\text{C}$ errors associated with P - T estimates from thermodynamic modeling³⁰. The errors for the $\Delta\log\text{FMQ}$ of the intermediate zones are calculated accounting for the slightly larger uncertainty in the P - T conditions and were calculated using upper and lower bounds for the possible P - T conditions (see further discussion in methods section and calculations in Supplementary Table 5).

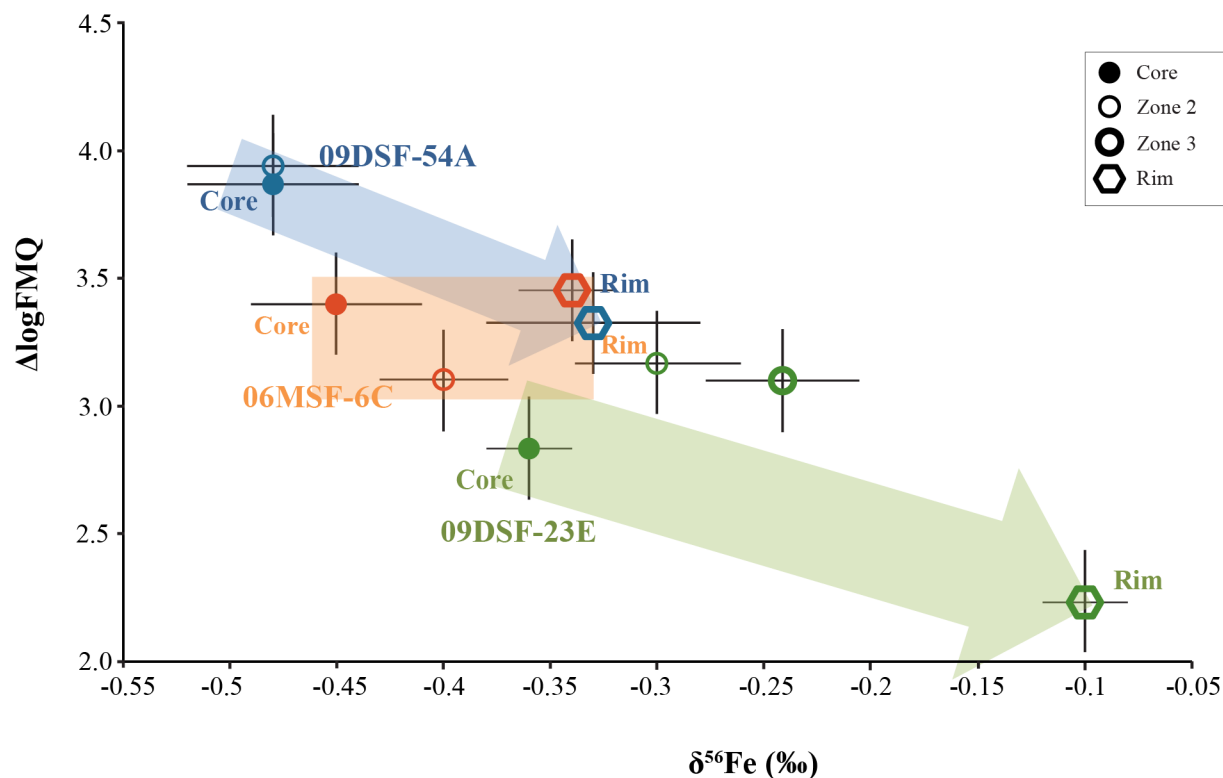


Figure 2-Iron isotope data, presented as $\delta^{56}\text{Fe}$ values, plotted against the $\Delta\log\text{FMQ}$ values for each zone (core, intermediate zones, rim). 09DSF-54A is plotted in blue, 09DSF-23E in green, and 06MSF-6C in orange. Each $f\text{O}_2$ data point represents a composite of all epidote inclusion-garnet pairs in that zone for the garnet. The arrows show the general trends in the data from the core (diamond markers) to intermediate zones (square markers) to garnet rims (circle markers). Error calculations for the $\delta^{56}\text{Fe}$ data are the two-standard deviation of four isotopic analysis for each sample. All error for $\Delta\log\text{FMQ}$ are ± 0.2 log units based on $\pm 1\text{kbar}$ and $\pm 40^\circ\text{C}$ error associated with P - T estimates from thermodynamic modeling³⁰.

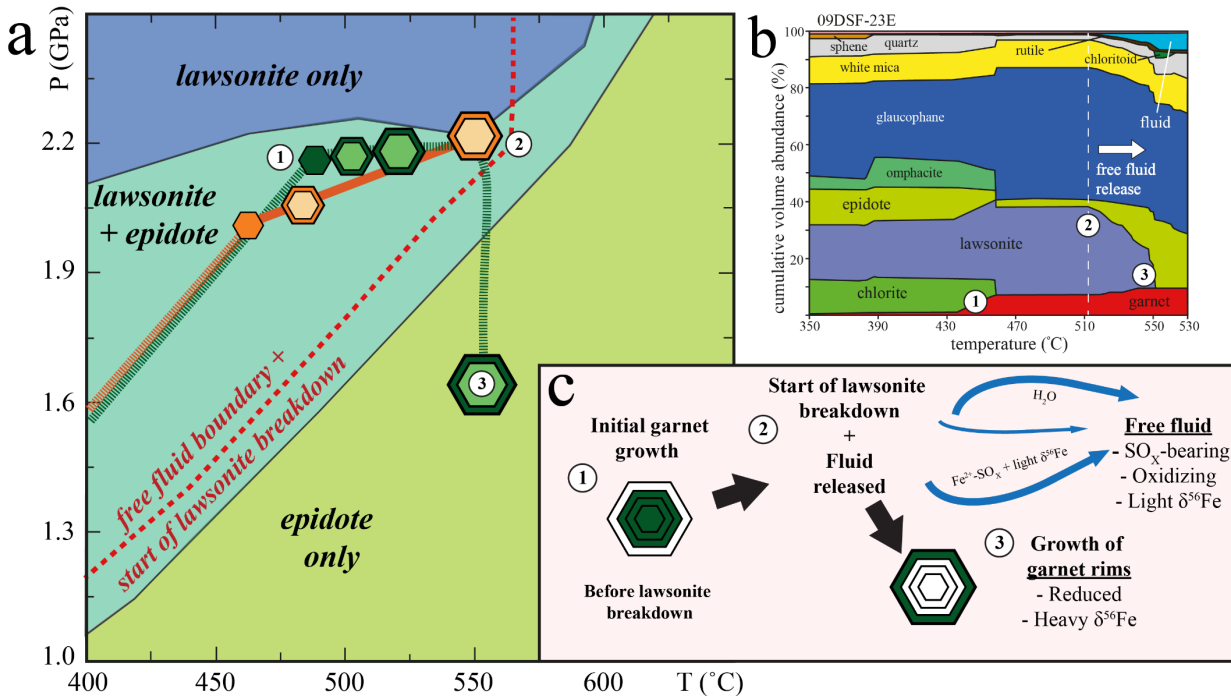


Figure 3 – a) Pressure-temperature (P - T) diagram showing P - T path during garnet growth for samples 09DSF-23E (green) and 06MSF-6C (orange). P - T path between garnet core and rim for sample 09DSF-23E is based on Sifnos P - T paths by Dragovic et al., (2012), Dragovic et al., (2015) and Groppo et al., (2009). The cartoon garnet zone symbols along the P - T path show the approximate P - T conditions at which these zones are interpreted to grow. Conditions of garnet growth for sample 09DSF-54A (not shown) is very similar to that for 09DSF-23E. Phases are labeled for fields showing P - T conditions where epidote, lawsonite, and lawsonite + epidote are stable. **b)** Cumulative modal mineral volume abundance (%) for sample 09DSF-23E along the prograde and retrograde P - T path given in the inset of Figure 3a. The onset of lawsonite breakdown releases a free fluid phase, shown as the light blue field and marked by the white dashed line at $\sim 515^\circ\text{C}$. **c)** Cartoon showing conditions for sample 09DSF-23E at labeled points 1, 2, and 3 on the P - T and cumulative modal abundance diagrams (Fig. 3a and 3b).

Acknowledgements

E.F.B. acknowledges support from NSF grants EAR-0547999 for sample collection and PIRE-1545903 for support during this project. E.I. was supported as a PDRA on ERC starting grant *PRISTINE*: 637503 awarded to Frédéric Moynier (IPG Paris).

Author Contributions

A.R.G. is responsible for the oxybarometry calculations, clean-lab preparation and analysis of Fe isotope compositions, and wrote the paper. E.I. performed Fe isotope compositional analysis and contributed to method development. B.D. is responsible for *P-T* modeling. P.G.S. performed clean-lab preparation, oxybarometry calculations, and method development. E.F.B. and K.B. contributed in designing the project. All authors contributed to analysis and interpretation of data and editing of the manuscript.

Author Information

Reprints and permissions information is available at www.nature.com/reprints. Correspondence and requests for materials should be addressed to A.R.G. (gerrits@bc.edu) or E.F.B. (ethan.baxter@bc.edu). All authors declare no competing interests.

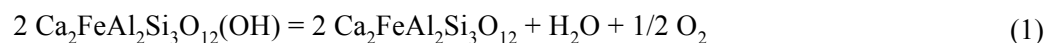
Methods

Oxygen fugacity, iron isotope, and thermodynamic modeling methods used in this study are presented below for samples 09DSF-23E, 09DSF-54A, and 06MSF-6C. All three samples are metabasalts collected from Sifnos, Greece. GPS locations for each sample are as follows: 09DSF-23E- N 37° 01.598', E 24° 39.396', 09DSF-54A- N 37° 00.930', E 24° 39.360', and 06MSF-6C- N 37° 01.561', E 24° 39.452'.

Oxygen Fugacity Calculations

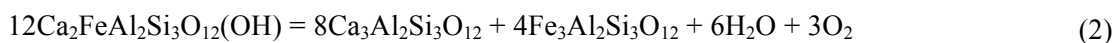
Oxygen fugacity methods and calculations are based on the oxygen barometer chemistry of Donohue & Essene (2002) utilizing the THERMOCALC program and thermodynamic database of Holland and Powell (1998). To ensure epidote inclusions are suitable for use in garnet-epidote oxygen barometer calculations, care was taken to identify primary epidotes, rather than compositionally patchy epidotes that reflect pseudomorphs after lawsonite. Epidote inclusions used in oxybarometry calculations (Supplementary Figure 2, Supplementary Figure 3, and Supplementary Figure 4) are in equilibrium with the surrounding garnet and show little to no cation zonation in BSE analysis. Epidote inclusions interpreted to be lawsonite pseudomorphs shows cation zonation visible in BSE and are accompanied by either paragonite or albite, representing breakdown products of lawsonite, (Supplementary Figure 5) and were avoided for this study.

Garnet and epidote endmember activities (Supplementary Table 3) were obtained at the appropriate P - T 's for each epidote-garnet pair (Supplementary Tables 1, 5, 6, 7) by inputting major element compositions of garnet and epidote minerals into the AX program (Tim Holland, University of Cambridge). Mineral compositions were acquired using wavelength dispersive spectrometry (WDS) on a JEOL-JXA-8200 electron microprobe at the Massachusetts Institute of Technology (Supplementary Table 4). All spot analyses were carried out using an acceleration voltage of 15kv, a current of 20nA, and approximate spot size of 5 μ m. Oxygen fugacity values (Supplementary Table 1) were calculated by inputting endmember activities of each epidote-garnet pair and the appropriate pressure and temperature into the thermodynamic modeling program, THERMOCALC^{31,32,33} using the equation:



Epidote ($\text{Ps}_{33}\text{Czo}_{67}$) Garnet ($\text{Alm}_{33}\text{Grs}_{67}$) Fluid

Which, can be rewritten to include grossular and almandine garnet end-members:



Epidote ($\text{Ps}_{33}\text{Czo}_{67}$) Grs garnet Alm garnet Fluid

Oxygen fugacity results are reported as $\Delta\log\text{FMQ}$, the difference between the calculated sample $f\text{O}_2$ and the FMQ buffer at a given P - T :

$$\Delta\log\text{FMQ} = (\text{Sample } f\text{O}_{2\ P-T} - \text{FMQ}_{P-T})$$

To obtain $\Delta\log\text{FMQ}$ values for each $f\text{O}_2$ value, the FMQ buffer was recalculated using the P - T conditions of each garnet-epidote oxybarometer pair used in $f\text{O}_2$ calculations.

The calculation of the Fe^{3+} (andradite) component from the electron microprobe analyses was carried out using the charge-balance method described in Quinn et al. (2016). As these charge-balance calculations of garnet compositions yield a low andradite component (<1.5% andradite component for garnet compositions in all three samples), garnet compositions used in oxygen fugacity calculations assume all iron in garnet is Fe^{2+} . The effects of Fe^{3+} substitution within garnet is minor, with the exception of within highly andraditic garnets (Donohue and Essene, 2000). The substitution of 15 mol% $\text{Fe}^{3+}/\Sigma\text{Fe}$, replacing Al in garnet, causes a shift of only ~ 0.1 log $f\text{O}_2$ units (Donohue and Essene, 2000). All iron in epidote mineral formulas used in oxygen fugacity calculations is assumed to be Fe^{3+} . Calculations assume a unit H_2O activity of 1 based on low salinity measurements of garnet fluid inclusions from Cycladic metabasalts³⁴ and the low modal abundance of carbonate. Errors in $\Delta\log\text{FMQ}$ (unless stated otherwise) are ± 0.2 log units based on the ± 1 kbar and $\pm 40^\circ\text{C}$ thermodynamic modeling error for P - T estimates presented in Palin et al. (2016).

Oxygen fugacity calculations for epidote-garnet pairs in core and rim zones use estimated pressures and temperatures of formation for each sample based on garnet isopleth thermodynamic modeling for samples 09DSF-23E (Supplementary Figure 7A&B), and 09DSF-54A (Supplementary

Figure 7C&D), and 06MSF-6C¹⁸. Without accurate P - T estimates for epidote inclusions in intermediate garnet zones, P - T 's were estimated using a P - T path from Sifnos, Greece with the prograde slope of Dragovic et al. (2012), and Dragovic et al. (2015). Thermodynamic modelling constraints suggest that the majority of garnet growth, likely including all of the intermediate zone growth, occurs at lower P - T conditions, shortly after the initial growth of the core (Figure 3b; Supplementary Figure 6). As a result, the P - T conditions chosen for the fO_2 calculations within the intermediate zones are close to those of the core, projecting a small distance along the estimated P - T path (Figure 3; Supplementary Table 1). To estimate the uncertainties on these calculated intermediate zone fO_2 values, both the uncertainties in the P - T calculations (± 1 kbar; $\pm 40^\circ\text{C}$) and the choice of P - T conditions were considered. Given that modelling shows very early garnet growth, it is plausible that all intermediate zone garnet growth occurred at the core conditions. Thus fO_2 values were calculated over a range of different P - T conditions, considering that garnet growth may have occurred anywhere between the core conditions and the chosen P - T conditions along the P - T path. The minimum bound on the fO_2 is calculated using the core conditions minus the P - T uncertainty (-1 kbar; -40°C) whilst the maximum bound is calculated using the chosen P - T conditions plus the P - T uncertainty (+1 kbar; +40°C) (see Supplementary Tables 5, 6 and 7). The resulting range of fO_2 values is considered to represent the uncertainty in these intermediate garnet zone calculations, shown in Figure 1c and Supplementary Figure 1. In practice, the resulting uncertainty in the fO_2 values is very similar to the ± 0.2 log units used for the rim and core points (Figure 1c; Supplementary Figure 1). Whilst there is a range in intermediate zone fO_2 for samples 09DSF-23E and 09DSF-54A, the main trend is that the fO_2 values clearly show a change from more oxidized garnet interiors to more reduced garnet rims in both samples independent of the choice of P - T path (Figure 1c and 2).

Iron Isotopes

Iron isotope ratios are reported as $\delta^{56}\text{Fe}$ and $\delta^{57}\text{Fe}$ using the IRMM-014 external standard with 2-standard deviation reported error (Supplementary Table 2).

$$\delta^{56}\text{Fe} = ((^{56}\text{Fe}/^{54}\text{Fe}_{\text{sample}})/(^{56}\text{Fe}/^{54}\text{Fe}_{\text{IRMM-014}})-1)*100$$

$$\delta^{57}\text{Fe} = ((^{57}\text{Fe}/^{54}\text{Fe}_{\text{sample}})/(^{57}\text{Fe}/^{54}\text{Fe}_{\text{IRMM-014}})-1)*100$$

Garnet powders used in iron isotope measurements were cleansed of inclusions and fully dissolved at Boston College (USA) before being passed through an iron exchange chromatographic procedure and analyzed for Fe isotope ratios at Durham University (UK). Growth zones were separated in individual garnet grains using the micro-drilling techniques presented in Pollington and Baxter (2011) to obtain three zones (core, zone 2, and rim) from samples 09DSF-54A and 06MSF-6C and four zones (core, zone 2, zone 3, and rim) from sample 09DSF-23E. Each garnet zone is then crushed to a 75-150 μm grain size and any visible inclusions were removed by handpicking and magnetic separation.

Samples were then put through a partial dissolution process, alternating dilute hydrofluoric and nitric acid steps to cleanse the garnet of inclusions. 10-50 mg of the picked garnet separate is heated at 120°C and sonicated in a closed beaker with 1 mL deionized Milli-Q water and 5-90 μL concentrated hydrofluoric acid added to 1 mL of Milli-Q water based on the starting amount of garnet for 120 minutes to dissolve inclusions. This acid mixture is then decanted and the garnet residue washed with 1mL of Milli-Q water four times. The residual garnet is then sonicated and heated at 120°C for 120 minutes in 2 mL 7 M nitric acid to completely dissolve any secondary fluorides. The nitric acid is decanted and the garnet residue is washed in 1mL 2 M nitric acid twice and 1mL Milli-Q water twice. This process is repeated until >50% of the original garnet has been dissolved. The inclusion-cleansed garnet residual is then fully dissolved using hydrofluoric acid, nitric acid, and hydrochloric acid.

Tests were conducted to explore potential Fe isotope fractionation during the partial dissolution process described above. Pure gem quality garnets with no visible inclusions from Mason Mountain Mine, North Carolina were crushed and subjected to various partial dissolution procedures. To test potential fractionation due to the acids used, garnet was partially dissolved separately in 7 M nitric, concentrated HF acid, and was also subjected to the full partial dissolution procedure described above. The resulting $\delta^{56}\text{Fe}$ compositions are all within error between pure garnet with no partial dissolution

(0.015 ± 0.046), garnet after partial dissolution cleansing in nitric acid (0.085 ± 0.028), garnet after partial dissolution cleansing in HF and nitric acid (0.08 ± 0.05), and garnet subjected to the full nitric-HF multi-stage partial dissolution technique (0.06 ± 0.033). While the starting garnet may not have been perfectly pure, the partial dissolution cleansing removed those inclusions (with lower $\delta^{56}\text{Fe}$) leaving behind a pure garnet with higher $\delta^{56}\text{Fe}$. Importantly, after this initial stage of partial dissolution cleaning, all subsequent steps to further treat the garnets yielded identical $\delta^{56}\text{Fe}$. This indicates the success of the method in removing the effects of non-garnet inclusions, but not altering the $\delta^{56}\text{Fe}$ of the pure garnet itself. Based on these results, the HNO_3 -HF multi-step partial dissolution was deemed appropriate to cleanse garnet of inclusions without fractionating iron isotope compositions. All garnet separates used in this study were subject to identical cleansing and preparation procedure. Sample drilling, crushing, and the partial and full dissolution processes were completed in the clean lab at Boston College.

Iron isotope measurements of the minerals were analyzed at Durham University between August and October 2017. The quantitative purification of Fe from the matrix elements was achieved using a protocol adapted from Dauphas et al. (2004). In this method 1.2 ml of BioRad AG1-X8 (200-400 mesh) anion exchange resin was packed onto 11.5 ml total capacity polypropylene columns, which was cleaned with passes of 10 ml MQ H_2O and 10 ml 6 M HCl repeated 4 times each. The resin was preconditioned with 2 ml of 6 M HCl and the sample loaded onto the column in 250 μl of 6 M HCl. The matrix was eluted from the retained Fe species by adding 8 ml of 6 M HCl and discarded. Iron was quantitatively recovered from the column by adding 9 ml 0.4 M HCl, and subsequently collected into clean 15 ml Savillex Teflon beakers. The pure Fe solution was evaporated to dryness and brought back into solution in 2 ml of 0.5 M HNO_3 prior to analysis by mass spectrometry. Prior calibration of this chromatographic ion exchange protocol demonstrated that the recovered Fe fraction was devoid of any isobaric elements (namely Cr and Ni) and totaled >99% of the Fe loaded into the column.

Iron isotope abundances were measured on a Thermo Scientific Neptune Plus MC-ICP-MS at Durham following the procedure of Weyer and Schwieters (2003). The instrument was run in medium-

resolution mode which gave a typical mass resolving power of ~ 6500 , adequate to discriminate between the $^{40}\text{Ar}^{14}\text{N}^+$, $^{40}\text{Ar}^{16}\text{O}^+$ and $^{40}\text{Ar}^{16}\text{OH}^+$ polyatomic species that are isobaric on the $^{54}\text{Fe}^+$, $^{56}\text{Fe}^+$, and $^{57}\text{Fe}^+$ masses respectively. Samples were introduced to the plasma interface using an Elemental Scientific SIS quartz spray chamber coupled with a PFA 50 $\mu\text{l}/\text{min}$ nebulizer. All of the Fe masses were collected, as were $^{53}\text{Cr}^+$ and $^{60}\text{Ni}^+$, in the movable faraday collectors, mounted within the back end of the instrument. $^{53}\text{Cr}^+$ and $^{60}\text{Ni}^+$ were used to correct, using the natural abundances, for any isobaric interference from these elements on the $^{54}\text{Fe}^+$ and $^{58}\text{Fe}^+$ masses. In all cases this correction had no effect on the calculated ratio as Cr and Ni were quantitatively removed from the sample solution prior to analysis by column chemistry. Instrumental mass bias was corrected using standard sample bracketing, where IRMM-014 was used as the bracketing standard. Precision and accuracy was assessed by measuring both an in-house secondary reference solution (Durham FeWire) and an external geo-reference material (USGS BIR 1). A total of 81 Durham FeWire analyses gave a mean of $\delta^{56}\text{Fe}$ of $+0.23 \pm 0.04 \text{ ‰}$ and a $\delta^{57}\text{Fe}$ of $+0.37 \pm 0.06 \text{ ‰}$ ($n=81$). Two aliquots of the BIR-1 geo-reference material were processed through two different batches of chemistry and analyzed a total of 4 times each. This gave an average $\delta^{56}\text{Fe}$ of $+0.06 \pm 0.028 \text{ ‰}$ and a $\delta^{57}\text{Fe}$ of $+0.09 \pm 0.021 \text{ ‰}$, which is in excellent agreement with published values for this standard^{38,39,40}. Total procedural blank yielded $<6\text{ng}$ Fe, which is negligible when compared to the total amount of Fe processed through the columns. The Fe isotope data for the samples analyzed as part of this study are reported in Supplementary Table 2 with error of two-standard deviation of four isotopic analyses for each sample.

Thermodynamic Modeling

To constrain the P - T conditions for garnet growth and the evolution of the metamorphic mineral assemblage during progressive subduction, P - T pseudosections and mineral modal plots were constructed using the thermodynamic program *Perple_X* (version 6.7.5)⁴¹ and the ‘ds 5.5’ update to the Holland and Powell (1998) internally-consistent dataset. The chemical system $\text{MnO-Na}_2\text{O-CaO-K}_2\text{O-FeO-MgO-Al}_2\text{O}_3\text{-SiO}_2\text{-H}_2\text{O-TiO}_2\text{-Fe}_2\text{O}_3$ (MnNCKFMASHTO) was used for all modelling. The following activity-

composition models were used for phases involving solid solution: pyroxene and amphibole⁴², garnet⁴³, white mica^{44, 45}, chlorite⁴⁶, feldspar⁴⁷, epidote and chloritoid³¹, spinel⁴⁸, ilmenite⁴⁹, and carbonates⁵⁰. In all the calculations, quartz, lawsonite, rutile, kyanite, and sphene were assumed to be pure, with phase equilibria calculations run in fluid-undersaturated conditions (see discussion below). Fe₂O₃ contents for the bulk compositions were evaluated by combining the average composition of phases with their respective volume abundances. Ferric iron contents of mineral phases were estimated from electron microprobe analyses using the AX program (Tim Holland, University of Cambridge).

Bulk compositions used for all phase equilibria calculations are shown in Supplementary Table 3, along with Fe³⁺/ΣFe (by mole fraction) used for each sample. Whole rock compositions were used in calculation of the *P-T* conditions of garnet growth initiation (garnet cores). As garnet is chemically zoned in both samples and the sequestration of components in zoned crystals can have a significant effect on both the effective composition of the rock and the resultant mineralogy⁵¹, independent bulk compositions of rock matrices were obtained by physical separation of garnet crystals from a whole rock volume. All bulk compositions (whole rocks and matrices) were determined by X-ray fluorescence (XRF) spectroscopy using a Phillips 2404 XRF vacuum spectrometer at Franklin and Marshall College.

Path dependent forward models take into account the continuous fractionation of garnet and water, following Baxter and Caddick (2013), with a sequence of regularly spaced *P-T* increments, where at each increment, the composition and modal abundance of all stable phases is predicted. The models were run at 0.5°C increments, with variable pressure increments. The *P-T* paths used for this modelling (Fig. 3A) were chosen based on the individual *P-T* gradients derived from Dragovic et al. (2015), also utilizing additional *P-T* constraints from Dragovic et al. (2012). The whole rock compositions were used as the initial bulk compositions for the phase fractionation calculations. The initial fluid contents for the phase fractionation calculations were determined based on repeat phase fractionation calculations to best model the observed mineralogy (of garnet inclusions and matrix) and volumetric mineral abundances. In order to reproduce the observed mineralogy, including the stable coexistence of lawsonite and epidote

during initial garnet growth, fluid undersaturated conditions were required. The initial fluid contents chosen for modelling of samples 09DSF-23E, 09DSF-54A, and 06MSF-6C are 6.0%, 4.0%, and 2.0%, respectively. Fluid in samples 09DSF-23E and 09DSF-54A were considered to be a fixed fluid H₂O–CO₂ compositions of 1 mol.% CO₂ – 99 mol.% H₂O (09DSF-23E) and 10 mol.% CO₂ – 90 mol.% H₂O (09DSF-54A). Fluid in sample 06MSF-6C was considered to be pure H₂O. These fluid compositions were estimated based on petrographic observations.

P-T pseudosections were calculated for the *P-T* range of 1.0-2.5 GPa and 400-650°C using the same *a-x* models listed above. The bulk composition used for the pseudosection modelling of each sample represents the effective bulk composition (garnet and water fractionated) calculated at 500°C along the phase fractionation path. The fluid contents used for the pseudosections that estimate the *P-T* of garnet crystal cores are the same as those used as the initial fluid content for the phase fractionation calculations. For the pseudosections that estimate the *P-T* conditions of garnet crystal rims, the fluid content was based on predictions from the phase fractionation calculations for the remnant fluid content at the assumed *P-T* conditions of garnet rim growth (3.0% for 09DSF-23E and 2.7% for 09DSF-54A). An iterative analysis of fluid content resulted in broadly similar *P-T* pseudosections and predicted garnet rim *P-T* conditions.

Rock descriptions

Sample 09DSF-23E

A complete petrographic description of sample 09DSF-23E can be found in Brooks et al. (2019). Sample 09DSF-23E is a garnet-epidote blueschist that contains large (cm-sized), euhedral garnet crystals along with large (several mm-sized) rhombohedral crystals of epidote. The remaining rock matrix consists of glaucophane, phengite, quartz, rutile, calcite, apatite, and trace albite and ilmenite. Glaucophane, phengite and elongate rutile grains define the foliation. The cores of garnet crystals are inclusion-rich, consisting of omphacite and quartz, with minor chlorite, phengite, paragonite, epidote, apatite, rutile, and ilmenite. Garnet rims contain inclusions of glaucophane. Epidote inclusions in garnet occur in two

varieties; a) isolated subhedral inclusions that are regarded as primary epidote, and b) anhedral inclusions that are chemically zoned, always associated with albite and/or paragonite and are interpreted to be pseudomorphic after lawsonite.

The above observations reflect the characteristics of a blueschist-overprinted eclogite, wherein the peak pressure assemblage consists of garnet, Na-pyroxene (omphacite), glaucophane, phengite, epidote, quartz, rutile, and accessory phases. The blueschist overprint resulted in the growth of garnet rims, chemically zoned amphibole, rhombohedral epidote porphyroblasts, albite, and most notably the loss of matrix omphacite.

Sample 09DSF-54A

Sample 09DSF-54A is a garnet-epidote blueschist consisting of large, cm-sized garnet porphyroblasts and cm-sized rhombohedral epidote crystals. The rock matrix is dominated by glaucophane, with lesser amounts of phengite, Na-pyroxene (aegerine), quartz, and titanite. Glaucophane and phengite define the foliation. Garnets are inclusion-rich, comprised of Na-pyroxene (aegerine and jadeite), phengite, epidote, paragonite, quartz, and rutile. As in sample 09DSF-23E, epidote occurs as a primary phase and in association with albite and/or paragonite, interpreted to be pseudomorphic after lawsonite.

Sample 09DSF-54A is regarded as a partially blueschist-overprinted eclogite. The peak eclogite assemblage consists of garnet, Na-pyroxene (aegerine and jadeite), phengite, epidote, quartz, and rutile. The blueschist overprint is only partial, as Na-pyroxene, a prograde to peak phase, has not been fully replaced by lower pressure re-equilibration. The partial blueschist overprint is comprised of glaucophane, rhombohedral epidote porphyroblasts, lower-Si phengite, and the replacement of rutile by titanite.

Sample 06MSF-6C

A complete petrographic description of sample 06MSF-6C can be found in Dragovic et al. (2012). Sample 06MSF-6C is a garnet-epidote blueschist containing cm-sized porphyroblasts of garnet and mm-sized rhombohedral crystals of epidote crosscutting the matrix foliation. Garnet contains inclusions of quartz, Na-pyroxene (jadeite), glaucophane, chloritoid, paragonite, phengite, and rutile.

Unlike the above two samples, epidote was found as inclusions in garnet solely as pseudomorphic after lawsonite in garnet mantles and rims. Rare lawsonite was found as inclusions in garnet cores. The rock matrix is defined by glaucophane and white mica (both paragonite and phengite), but also consists of rhombohedral epidote, rutile, quartz, and anhedral masses of jadeitic pyroxene.

Sample 06MSF-6C is interpreted to be a transitional blueschist to eclogite facies lithology. The peak assemblage is comprised of garnet, jadeite, glaucophane, paragonite, phengite, quartz and rutile. Matrix re-equilibration during the early stages of exhumation resulted in growth of rhombohedral epidote, paragonite and phengite that crosscuts the foliation.

Data Availability

The authors declare that the data generated or analyzed during this study are included in this published article and its Supplementary Information files.

Methods References

31. Holland, T.J.B. & Powell, R. An internally consistent thermodynamic data set for phases of petrological interest. *J. Metamorph. Geol.* **16**, 309-343 (1998).
32. Powell, R. & Holland, T.J.B. An internally consistent dataset with uncertainties and correlations: 3. Applications to geobarometry, worked examples and a computer program. *J. Metamorph. Geol.* **6**, 173-204 (1988).
33. Powell, R. & Holland, T. Optimal geothermometry and geobarometry. *Am. Mineral.* **79**, 120-133 (1994).
34. Barr, H. Preliminary fluid inclusion studies in a high-grade blueschist terrain, Syros, Greece. *Mineral. Mag.* **54**, 159-168 (1990).
35. Pollington, A.D. & Baxter, E.F. High precision microsampling and preparation of zoned garnet porphyroblasts for Sm-Nd geochronology. *Chem. Geol.* **281**, 270-282 (2011).
36. Dauphas, N., et al. Chromatographic separation and multicollection-ICPMS analysis of iron. Investigating mass-dependent and-independent isotope effects. *Analytical Chem.* **76**, 5855-5863 (2004).
37. Weyer, S. and Schwieters, J.B. High precision Fe isotope measurements with high mass resolution MC-ICPMS. *International Journal of Mass Spectrometry*, **226**, 355-368 (2003).
38. Millet, M.A., Baker, J.A. and Payne, C.E. Ultra-precise stable Fe isotope measurements by high resolution multiple-collector inductively coupled plasma mass spectrometry with a ^{57}Fe - ^{58}Fe double spike. *Chem. Geol.* **304**, 18-25 (2012).
39. Hibbert, K.E.J., Williams, H.M., Kerr, A.C. and Puchtel, I.S. Iron isotopes in ancient and modern komatiites: evidence in support of an oxidised mantle from Archean to present. *Earth Planet. Sci. Lett.* **321**, 198-207 (2012).
40. Sossi, P.A., Halverson, G.P., Nebel, O. and Eggins, S.M. Combined separation of Cu, Fe and Zn

- from rock matrices and improved analytical protocols for stable isotope determination. *Geostandards and Geoanalytical Research*, **39**, 129-149 (2015).
41. Connolly, J.A.D. The geodynamic equation of state: what and how. *Geochem. Geophys. Geosyst.* **10**, 10 (2009).
 42. Diener, J.F.A. and Powell, R. Revised activity–composition models for clinopyroxene and amphibole. *J. Metamorph. Geol.* **30**, 131-142 (2012).
 43. White, R.W., Powell, R. and Holland, T.J.B. Progress relating to calculation of partial melting equilibria for metapelites. *J. Metamorph. Geol.* **25**, 511-527 (2007).
 44. Auzanneau, E., Schmidt, M.W., Vielzeuf, D. and Connolly, J.D. Titanium in phengite: a geobarometer for high temperature eclogites. *Contrib. Mineral. Petrol.* **159**, 1 (2010).
 45. Coggan, R. and Holland, T.J.B. Mixing properties of phengitic micas and revised garnet–phengite thermometers. *J. Metamorph. Geol.* **20**, 683-696 (2002).
 46. Powell, R., Holland, T.J.B.H. and Worley, B. Calculating phase diagrams involving solid solutions via non - linear equations, with examples using THERMOCALC. *J. Metamorph. Geol.* **16**, 577-588 (1998).
 47. Fuhrman, M.L. and Lindsley, D.H. Ternary-feldspar modeling and thermometry. *Am. Mineral.* **73**, 201–215 (1988).
 48. White, R.W., Powell, R. and Clarke, G.L. The interpretation of reaction textures in Fe - rich metapelitic granulites of the Musgrave Block, central Australia: constraints from mineral equilibria calculations in the system $K_2O-FeO-MgO-Al_2O_3-SiO_2-H_2O-TiO_2-Fe_2O_3$. *J. Metamorph. Geol.* **20**, 41-55 (2002).
 49. White, R.W., Powell, R., Holland, T.J.B. and Worley, B.A. The effect of TiO_2 and Fe_2O_3 on metapelitic assemblages at greenschist and amphibolite facies conditions: mineral equilibria calculations in the system $K_2O-FeO-MgO-Al_2O_3-SiO_2-H_2O-TiO_2-Fe_2O_3$. *J. Metamorph. Geol.* **18**, 497-512 (2002).
 50. Holland, T. and Powell, R. Activity–composition relations for phases in petrological calculations: an asymmetric multicomponent formulation. *Contrib. Mineral. Petrol.* **145**, 492-501 (2003).
 51. Marmo, B.A., Clarke, G.L. and Powell, R. Fractionation of bulk rock composition due to porphyroblast growth: effects on eclogite facies mineral equilibria, Pam Peninsula, New Caledonia. *J. Metamorph. Geol.* **20**, 151-165 (2002).
 52. Brooks, H.L., Dragovic, B., Lamadrid, H.M., Caddick, M.J., Bodnar, R., 2019. Fluid capture during exhumation of subducted lithologies: a fluid inclusion study from Sifnos, Greece. *Lithos*, 332-333, 120-134.
 53. Dragovic, B., Samanta, L., Baxter, E.F., Selverstone, J., 2012. Using garnet to constrain the duration and rate of water-releasing metamorphic reactions during subduction: An example from Sifnos, Greece. *Chemical Geology*, 314-317, 9-22.